LETTERS

nature cell biology

# Differentially oriented populations of actin filaments generated in lamellipodia collaborate in pushing and pausing at the cell front

Stefan A. Koestler[1], Sonja Auinger[1], Marlene Vinzenz[1], Klemens Rottner[2] and J. Victor Small[1,3]

**Eukaryotic cells advance in phases of protrusion, pause and withdrawal[1]. Protrusion occurs in lamellipodia, which are composed of diagonal networks of actin filaments, and withdrawal terminates with the formation of actin bundles parallel to the cell edge. Using correlated live-cell imaging and electron microscopy, we have shown that actin filaments in protruding lamellipodia subtend angles from 15–90° to the front, and that transitions from protrusion to pause are associated with a proportional increase in filaments oriented more parallel to the cell edge. Microspike bundles of actin filaments also showed a wide angular distribution and correspondingly variable bilateral polymerization rates along the cell front. We propose that the angular shift of filaments in lamellipodia serves in adapting to slower protrusion rates while maintaining the filament densities required for structural support; further, we suggest that single filaments and microspike bundles contribute to the construction of the lamella behind and to the formation of the cell edge when protrusion ceases. Our findings provide an explanation for the variable turnover dynamics of actin filaments in lamellipodia observed by fluorescence speckle microscopy[2] and are inconsistent with a current model of lamellipodia structure that features actin filaments branching at 70° in a dendritic array[3].**

Migrating cells exploit two properties of actin filaments to move: the property to polymerize and push (to effect protrusion) and the ability to slide with myosin II (to drive retraction). Protrusion is effected by lamellipodia[1,4], thin sheets of cytoplasm containing networks of actin filaments that have their fast growing plus-ends abutting the leading membrane[5]. Current ideas of how protruding lamellipodia are organized have come mainly from electron microscopic analysis of cells that show constant motility, in particular, the epidermal keratocyte[3,6]. From images obtained using a critical-point drying procedure for specimen preparation, a model of lamellipodium organization has been proposed that features a dendritic network of actin filaments with the Arp2/3 complex situated at 70° branch points[3,7,8].

In migrating cells, lamellipodia not only protrude, they undergo phases of protrusion, pause and withdrawal, the latter often associated with ruffling[1]. Filopodia and related bundles embedded in the lamellipodia mesh, also referred to as microspikes[4], contribute to these activities. To gain insight into the structural basis of changes in protrusive activity, we have developed procedures for correlating the local movements of lamellipodia (monitored by live-cell imaging) with their organization after negative-stain electron microscopy. Results obtained using this approach reveal filament arrangements and rearrangements in lamellipodia that are difficult to reconcile with the dendritic model. They also show how filament remodelling in lamellipodia may contribute to the construction of stationary cell edges and to the assembly of the cytoskeleton of the lamella region behind the lamellipodium[9].

Figure 1 shows the final frames of a video sequence (Supplementary Information, Movie 1) of a fast and steadily protruding B16 melanoma cell expressing green fluorescent protein (GFP)–actin and mCherry–VASP, before and after fixation on the light microscope (Fig. 1a, b) and an overview of the cell in the electron microscope (Fig. 1d). VASP (vasodilator-stimulated phosphoprotein) is a useful indicator of protrusion, as the intensity of lamellipodia-tip labelling is proportional to the protrusion rate[10]. The time between the final video frame and the fixation event was approximately 3 s. Scans of the GFP intensity across the lamellipodium (Fig. 1b, inset) in the main protruding zone (Fig. 1b, box) demonstrated that the gradient of actin fluorescence in the lamellipodium of the living cell was preserved by the fixation process. Frames of the video sequence in the boxed area in Fig. 1b are shown in Fig. 1c (upper panels), together with the velocity profile in this position (Fig. 1c, bottom panel). The mean protrusion rate over the terminal 60 s was 3.5 μm $min^{-1}$. Electron micrographs of the same region close to and 5 μm behind the lamellipodium front (Fig. 1d, small boxed regions) are shown in Fig. 2a and b (for an overview, see Supplementary Information, Fig. S1). The number of filaments crossing 1 μm lines drawn 0.2 μm

[1]Institute of Molecular Biotechnology, Austrian Academy of Sciences, Dr. Bohr-Gasse 3, 1030, Vienna, Austria. [2]Cytoskeleton Dynamics Group, Helmholtz Centre for Infection Research (HZI), Inhoffen Strasse 7, D-38124 Braunschweig, Germany.
[3]Correspondence should be addressed to J.V.S. (e-mail: vic.small@imba.oeaw.ac.at)

Received 19 November 2007; accepted 28 January 2008; published online 17 February 2008; DOI: 10.1038/ncb1692

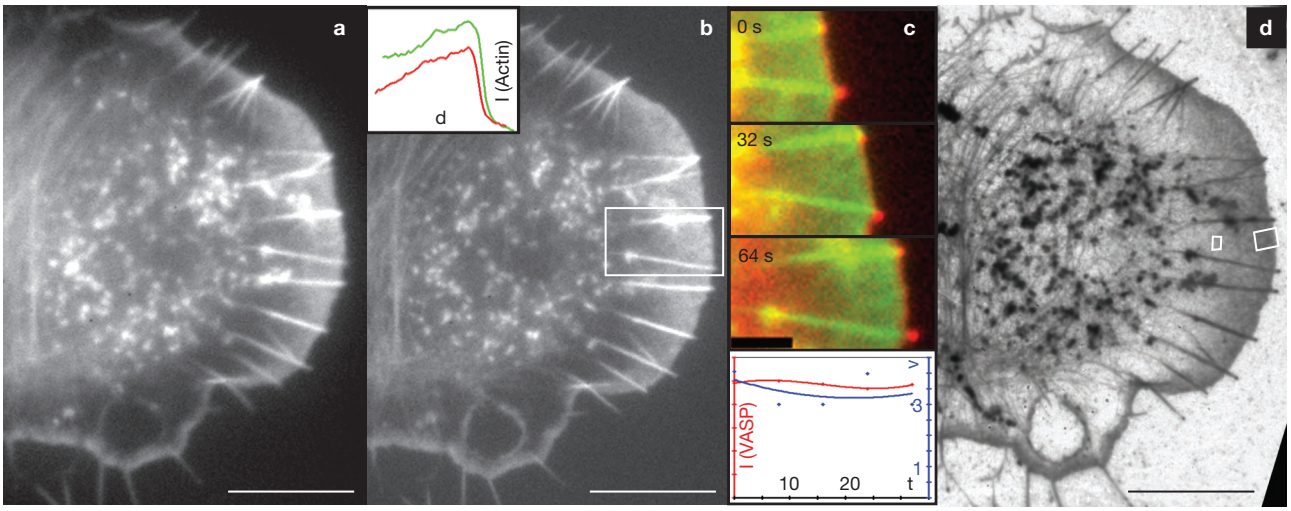


**Figure 1** Arrest of a steadily protruding lamellipodium and preservation of the actin gradient. (**a**) Final frame (GFP channel) of a video sequence showing a B16 melanoma cell expressing GFP–actin and mCherry–VASP. (**b**) Actin–GFP image of a cell fixed within 3 s after the last video frame shown in **a**. The inset shows intensity scans (I (Actin)) across the lamellipodium (boxed region) before (green line) and after (red line) fixation; d in the inset is the distance. (**c**) Upper panels: video sequence leading to fixation of boxed region in **b** (green, GFP–actin; red, mCherry–VASP). Lower panel: protrusion rate over the terminal period (*v*, μm min$^{-1}$; blue) and the relative mCherry–VASP intensity at the front edge of the lamellipodium (I (VASP); red). (**d**) Overview electron micrograph of the cell after negative staining. Bars are 10 μm (**a**, **b**, **d**) and 3 μm (**c**). See also Supplementary Information, Movie 1.

behind the cell front in this advancing lamellipodium averaged 90 ± 10. Particularly noteworthy was the wide angular distribution of filaments, from 15–90°, with respect to the cell edge (Fig. 2a, left inset). In a region 5 μm behind the front of the same lamellipodium (Fig. 1d, Fig. 2b, small box inset; Supplementary Information, Fig. S1), the filament density was lower (59 ±15 filaments μm$^{-1}$). In addition, there was an increase in the proportion of filaments at low angles to the cell front (Fig. 2b, inset). The gradient of filament density across the lamellipodium back to 3.5 μm from the front correlated with the gradient of actin–GFP intensity in the same position of the living and fixed cell (Fig. 2a, right inset) and revealed a drop in filament number of 11% over the first micron.

Figure 3a–e (Supplementary Information, Movie 2) shows a cell for which three regions of different protrusive activity are highlighted (Fig. 3b), with enlarged video frames in Fig. 3c–e. At position C (Fig. 3b), the protrusion rate (approximately 2 μm min$^{-1}$) and VASP intensity were more or less constant over the terminal 2 min (Fig. 3c, middle panel). Figure 3f shows the organization of actin filaments at the front of the lamellipodium in the same region of the cell. Further analysis (Fig. 3c, histogram, lower panel) showed an angular distribution of filaments in a region 0.2 μm from the cell front; notably, there was a wide distribution of angles down to 15°, as well as the presence of a small population of filaments subtending angles below 20° to the cell edge (Fig. 3f), which also extended up to the tip of the lamellipodium (arrow). The cell in Fig. 3 moved throughout the video sequence without a significant change in overall shape. Consequently, the radial protrusion rate decreased steadily from the advancing shoulders out to the lateral flanks. In position D (Fig. 3b), the rate of protrusion just prior to fixation was 1 μm min$^{-1}$ and the VASP label declined steadily over the terminal 2 min (Fig. 3d, middle panel). In this position, a large proportion of filaments was oriented at lower angles to the cell edge (Fig. 4a; see also histogram in Fig. 3d) and could be seen to originate from foci at the lamellipodium front. The same reorganization of filaments from the peak towards the flank was seen in equivalent positions of the lamellipodium on the opposite half of the cell (data not shown). At the extreme lateral flank of the same cell (position E, Fig. 3b, e) there was no net protrusion, but small fluctuations of the cell edge that ended in a minor retraction and complete loss of VASP label (Fig. 3E). Electron microscopy (Fig. 4b) showed that the lamellipodium at this position was approximately 0.5 μm wide and contained a major component of filaments oriented parallel to the cell edge, superimposed on a narrow band (0.2 μm wide) of divergent filament arrays and characteristic of early protrusions. Analysis of MTLn3 carcinoma cells, which migrate actively *in vitro* and *in vivo*[11], revealed essentially the same changes in filament organization between regions of protrusion and pause; namely, a shift in orientation of filaments to lower angles (some to below 15°) and, in addition, the appearance in pausing zones of a noticeable proportion of filaments with curved trajectories (Supplementary Information, Fig. S2). Slowing and pause were associated with a 30% reduction in filament numbers at the front (Fig. 3, positions C and D) of the B16 melanoma cell (Fig. 3f, inset).

According to their varied orientation to the cell front, actin filament tips must move laterally along the cell edge as they grow[12]. This lateral flow was reflected in the movement of microspike bundles, commonly embedded in protruding lamellipodia, of B16 melanoma cells (Supplementary Information, Fig. S3a–g and Movie 3). The angle that such bundles subtended with the cell front varied, ranging from 90° to below 10° (Supplementary Information, Fig. S3h), in the same range as observed for individual filaments. In addition, the proportion of microspikes at lower angles was higher in slowing and pausing lamellipodia when compared with continuously protruding ones (Supplementary Information, Fig. S3h). A direct consequence of this angular distribution was variation in the velocity of lateral movement of microspike tips along the cell edge and in the length of the bundles. Using photo-activatable-GFP (PA-GFP; Supplementary Information, Fig. S3e and Movie 3e), we showed that the polymerization rate in microspikes increased up to 15 μm min$^{-1}$ for those oriented at approximately 15° to the cell edge (Supplementary Information, Fig. S3i). Microspike bundles moved laterally in opposite directions and

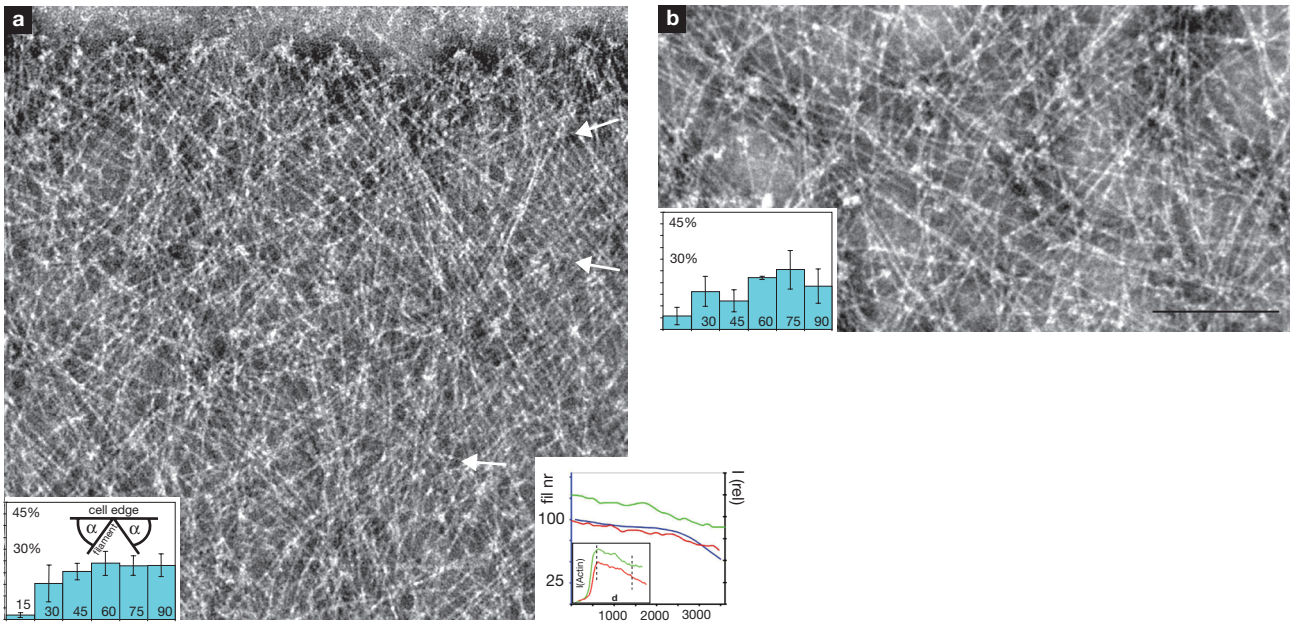


**Figure 2** Actin filaments are variably orientated in protruding lamellipodia. (**a**) Electron micrograph of the front region of the lamellipodium shown in Fig. 1b–d (peripheral zone boxed in Fig. 1d and Supplementary Information, Fig. S1). The histogram shows the angular distribution of filaments crossing a line (1 μm) drawn parallel to and 100 nm behind the front edge of the lamellipodium (mean of five adjacent regions; total of 451 filaments). Filaments diverged at variable angles from foci at the cell front. Arrows indicate some examples of filaments at low angles. (**b**) The region in the same lamellipodium, 5 μm behind the cell edge (inner region boxed in Fig. 1d and Supplementary Information, Fig. S1); histogram shows the angular distribution of filaments crossing a line (1 μm) parallel to the cell front (mean of four adjacent regions 5 μm from front edge; total of 236 filaments). Note the decrease in filament density and increase in the number of filaments at lower angles to the cell edge. Inset right in **a**: comparison of the fluorescence signal across the lamellipodium (Fig. 1b) with the actin filament density (per 1 μm of lamellipodium width) determined from electron micrographs taken from the region including Figs. 2a, b. The filament counts at 200 nm from the front were normalized to the peak of the fluorescence scan of the fixed cell (red). The fluorescence traces correspond to the signal between the dotted lines shown in the inset. Scale bar is 200 nm.

could be observed to cross each other (Supplementary Information, Fig. S3b and Movie 3b) or to fuse. One consequence of these bilateral movements was the generation of antiparallel arrays of actin filaments that formed bundles at the base of the lamellipodium, from where they entered the lamella and accumulated myosin (Supplementary Information, Fig. S3f and Movie 3f). Other microspikes contributed directly to the formation of retracting edges (Supplementary Information, Fig. S3a and Movie 3a). Although the lateral flow of microspikes could lead to their integration into the lamella with myosin, it was not dependent on myosin II, as shown by its persistence in the presence of the myosin II inhibitor blebbistatin (Supplementary Information, Fig. S3g and Movie 3g). In the short term (within 2–10 min), blebbistatin (50–100 μM) induced an increase in the rate of lamellipodia protrusion by a factor of 1.5–3 and an increase in the lamellipodium width (Supplementary Information, Fig. S3j, k), analogous to observations on immobilized *Aplysia californica* growth cones[13].

The negative staining method, as used here and in earlier studies (reviewed in ref. 14), has the advantage that linearity of filaments within the delicate meshwork of the lamellipodium is maintained and the dorsal and ventral arrays of actin are included in the electron microscope images. For the first time, we were thus able to relate the angular distributions of filaments and filament densities to the history of protrusion. Our direct measurements indicate that around 100 filaments per micron are utilized during protrusion. This value is approximately half that estimated indirectly by comparison of the fluorescence intensity of phalloidin-labelled single actin filaments with that of phalloidin-labelled lamellipodia of fixed 3T3 fibroblasts[15]. From the present and earlier studies, it is clear that the filament density in lamellipodia does not determine the protrusion rate, as it differs little between keratocytes that can move at 15 μm $min^{-1}$ (ref. 6) and B16 melanoma and MTLn3 adenocarcinoma cells protruding five times more slowly. Correspondingly, we found that slowing of the cell edge was not accompanied by a significant decrease in filament density. Instead, there was a consistent increase in the number of filaments oriented at a low angle to the cell edge. The wide angular distribution of filaments, all with their plus-ends forward, indicate that there is a spread of polymerization rates, with filaments at low angles growing fastest to keep up with the front. The factors determining this variation in rate are unknown, but may be influenced by a type of force-dependent feedback mechanism[16], caused by progressively lower resistance to filament growth at lower angles. We suggest that the transition from protrusion to pause is signalled by the net local downregulation of actin plus-end polymerization complexes, but with some polymerization complexes being downregulated more than others. In this model, actin filaments polymerizing slowest act as a brake on protrusion through tethering with the leading membrane, analogous to the tethering of actin filaments to beads in mimetic models of cell motility[17,18]. Other, faster growing filaments must re-orient their trajectory, relative to the front edge, to grow. This causes an increase in the population of filaments at lower angles (Supplementary Information, Movie 4). If pause persists, more filaments become parallel to the cell front; some may also detach and move backwards with retrograde flow to the base of the lamellipodium, as observed with microspike bundles (Supplementary Information, Fig. S3c, Movie 3c; ref. 19).

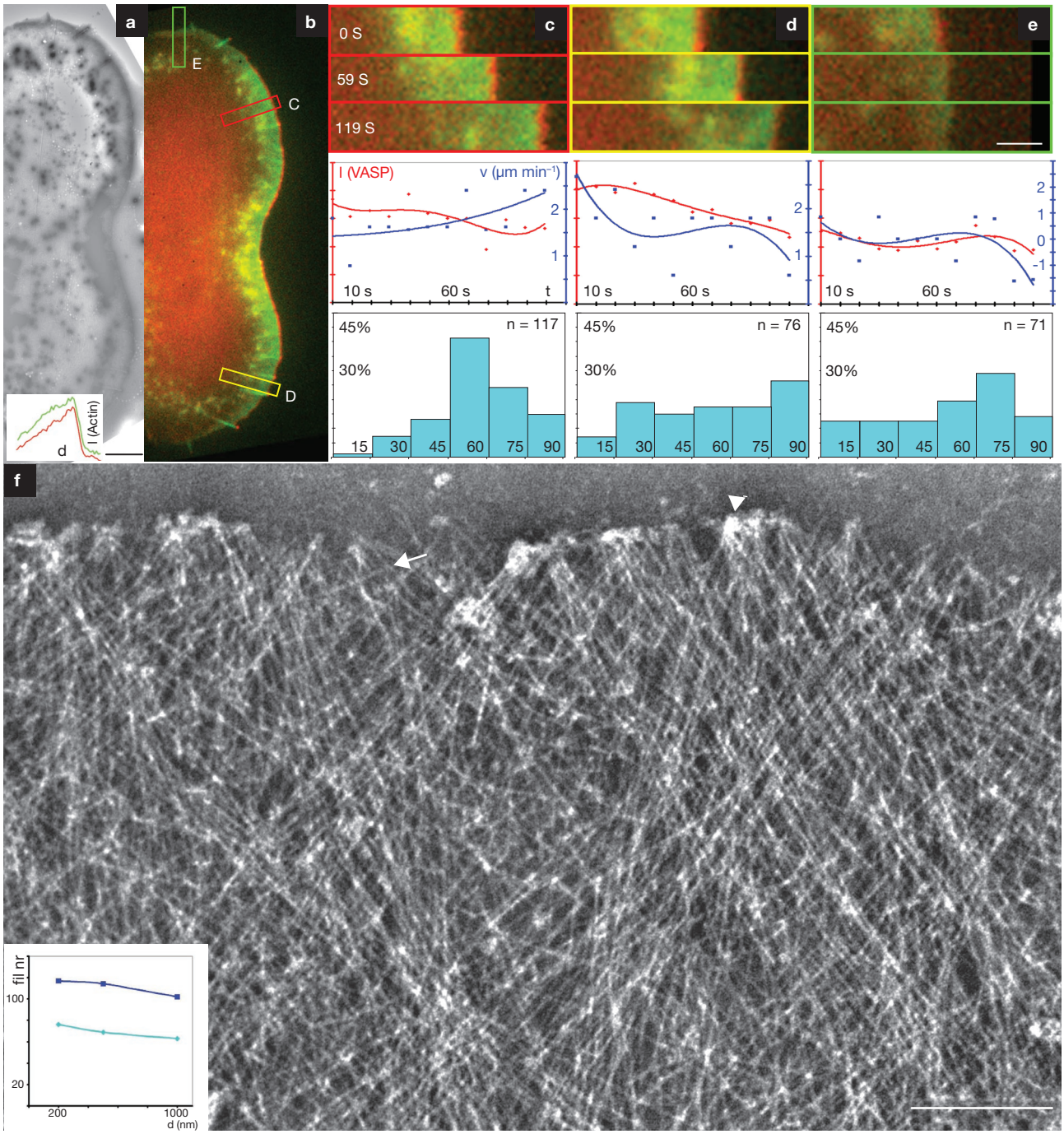


**Figure 3** Actin filaments reorganize during the transition from protrusion to retraction. (**a**, **b**) Overview electron micrograph (**a**) and terminal video frame (**b**) of a B16 melanoma cell transfected with GFP–actin and mCherry–VASP (see Supplementary Information, Movie 2). Inset in **a**: intensity scans of GFP–actin fluorescence across the lamellipodium in a protruding region before (green) and after (red) fixation showing retention of actin-density gradient. (**c**–**e**) Upper panels show terminal video sequences of boxed regions **C**, **D** and **E** marked in **b** (green, GFP–actin; red, mCherry–VASP); Middle panels, protrusion rate (*v*, μm min$^{-1}$, blue) and relative VASP intensity at lamellipodium front (I (VASP), red) as a function of time (*t*, s); Lower panels, histograms of the angular distribution of filaments relative to the cell front for the corresponding electron micrographs (**f** and Fig. 4a, b), measured at 200 nm from cell edge across a line (1 μm). '*n*' is the number of filaments measured; numbers in bars indicate the angle to the cell edge. (**f**) Electron micrograph of front region of protruding lamellipodium in boxed region **c**. Note partial grouping of filaments oriented at high angles to the front (arrowhead), as well as a subpopulation of individual filaments at shallow angles (arrow; see also histogram in **c**). Inset: comparison of filament counts back to 1 μm in this part of the lamellipodium (violet) with the pausing region shown in Fig. 4a (light blue). Scale bars are 5 μm (**a**), 2 μm (**c**–**e**) and 200 nm (**f**).

The advance of the lamellipodium depends on a balance between the rate of actin polymerization and the rate of retrograde flow. Recent findings on immobilized *Aplysia* growth cones indicate that a component of retrograde flow is driven by myosin II activity in the lamella[13], consistent with our observation of an increase in lamellipodia protrusion rate in B16 cells treated with blebbistatin. Pausing in lamellipodia may therefore

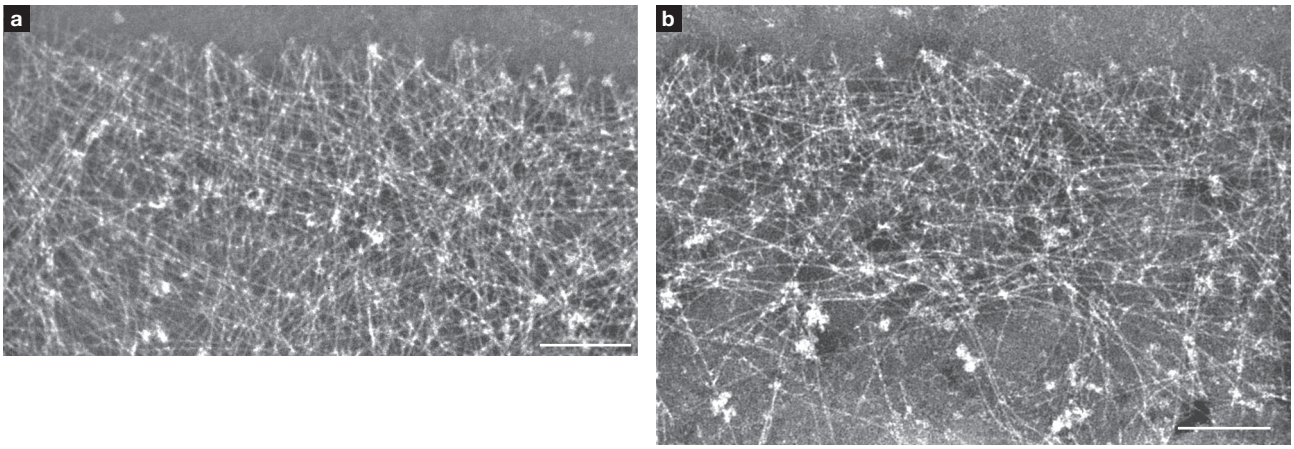


**Figure 4** Slowing and pause is associated with an increase in the number of filaments at shallow angles to the lamellipodium front. (**a**) Electron micrograph of region D in Fig. 3b, where the protrusion rate had slowed down to 1 μm $min^{-1}$ at the point of fixation (Fig. 3d, middle panel,). Note the prevalence of filaments at low angles to the cell edge (see also Fig. 3d histogram, lower panel) and that these filaments originate from foci at the lamellipodium front. (**b**) Electron micrograph of region E in Fig. 3b, on the lateral flank of the cell where protrusion had ceased (Fig. 3e, middle panel). Note the dominance of filaments parallel to the cell edge (see also Fig. 3e histogram, bottom panel). Scale bars are 200 nm.

be explained by a reduction in the net forward polymerization rate at filament plus-ends to the rate component of retrograde flow contributed by myosin–actin interactions at the base of the lamellipodium. An analogous situation is apparent in fish keratocyte lamellipodia, for which protrusion is maximal at the front and reduces to zero at the flanks. At the front there is minimal retrograde flow[20], whereas at the flanks, retrograde flow is maximal; this can be explained as the combined contributions of actin polymerization at the membrane and the myosin-dependent withdrawal of filaments into the cell body[20].

On the basis of this study, we propose a simple model in which different ramifications of filament reorganization in the lamellipodium lead to the contribution of anti-parallel filament arrays, including arcs[9,12,21], to the lamella during protrusion (Fig. 5a) and to the cell edge during retraction (Fig. 5b); in both cases filament arrays are produced to allow the formation of contractile assemblies with myosin. In this scheme, there is a gradation of filament lengths in lamellipodia according to the angular distribution and the drop in actin filament density away from the front. From elementary geometric considerations, filaments oriented at 15° to the cell edge that extend to the rear of the lamellipodium will be three times longer than those oriented at 55°. For a lamellipodium of 3 μm in width, this would correspond to maximum filament lengths of 11.6 μm and 3.7 μm, respectively (disregarding those that extend further into the lamella). During persistent pause, depolymerization from filament minus-ends will eliminate shorter filaments at higher angles to the cell edge first, leaving the longer filaments shorter, but still long enough to form a parallel bundle. We assume that the association of these latter filaments with tropomyosin protect them from further depolymerization[22] and promote their interaction with myosin to consolidate the cell edge. Rather than being static, filaments that enter the lamella continue to turnover (Supplementary Information, Fig. S3e, Movie 3e; ref. 2), so that their lamellipodia precursors can be viewed as seeds of the lamella cytoskeleton.

The currently popular dendritic network model of lamellipodium protrusion[7,8,23] features 70° Y-junctions within 20–50 nm of each other in the actin network[3] and branched filament segments behind the cell front that are capped at their plus ends. The model derives from analysis of electron micrographs of cytoskeletons prepared by the critical-point drying method[3] and extrapolation of data showing the ability of the Arp2/3-complex to induce the branching of actin filaments *in vitro*[24,25]. Definitive proof of whether or not branches exist at all in lamellipodia will need to come from cryo-electron tomography, to counter any arguments about artefacts induced by specimen preparation[26] and three-dimensional organization. The feasibility of visualizing actin filaments in vitreously frozen *Dictyostelium discoideum* amoebae has been shown previously[27] and the challenge now is to combine this methodology with information about the motile activity of the imaged regions. Nevertheless, we already show that there is no regular angle of 70° between filaments at the front of a protruding cell edge. And with a primary fixation stronger than that used previously[3], we found no evidence of actin-filament branches.

From analysis of actin-filament turnover by fluorescence speckle microscopy[2,28] and lamellipodia spreading dynamics[29], it has been concluded that the lamellipodium 'surfs' on top of the lamella underneath. Our results indicate, however, that all filaments in the lamellipodium originate from nucleation centres at the tip, with no superposition of the lamellipodium network on another array beneath; the lamellipodium and lamella are spatially and structurally distinct, although coupled at their boundaries[9], where myosin engagement begins. In addition, we provide an alternative explanation for the different populations of actin speckles observed in lamellipodia[2]. The longest-lived speckles can be explained as belonging to the long filaments that extend to the base of the lamellipodium and the short-lived speckles to those that terminate within the lamellipodium network. The possibility exists that a variable rate of treadmilling of individual filaments and bundles at different angles also contributes to the variability in retrograde flow rate. This idea could be tested by electron microscopy in conjunction with speckle microscopy[2] or spatiotemporal image correlation microscopy[30].

In conclusion, correlated live-cell imaging and electron microscopy has revealed a shift in the angular distribution of filaments in lamellipodia according to protrusive activity. These findings shed new light on the way actin is used to drive cell motility and also prompts a re-evaluation of current ideas about actin-filament organization in lamellipodia.

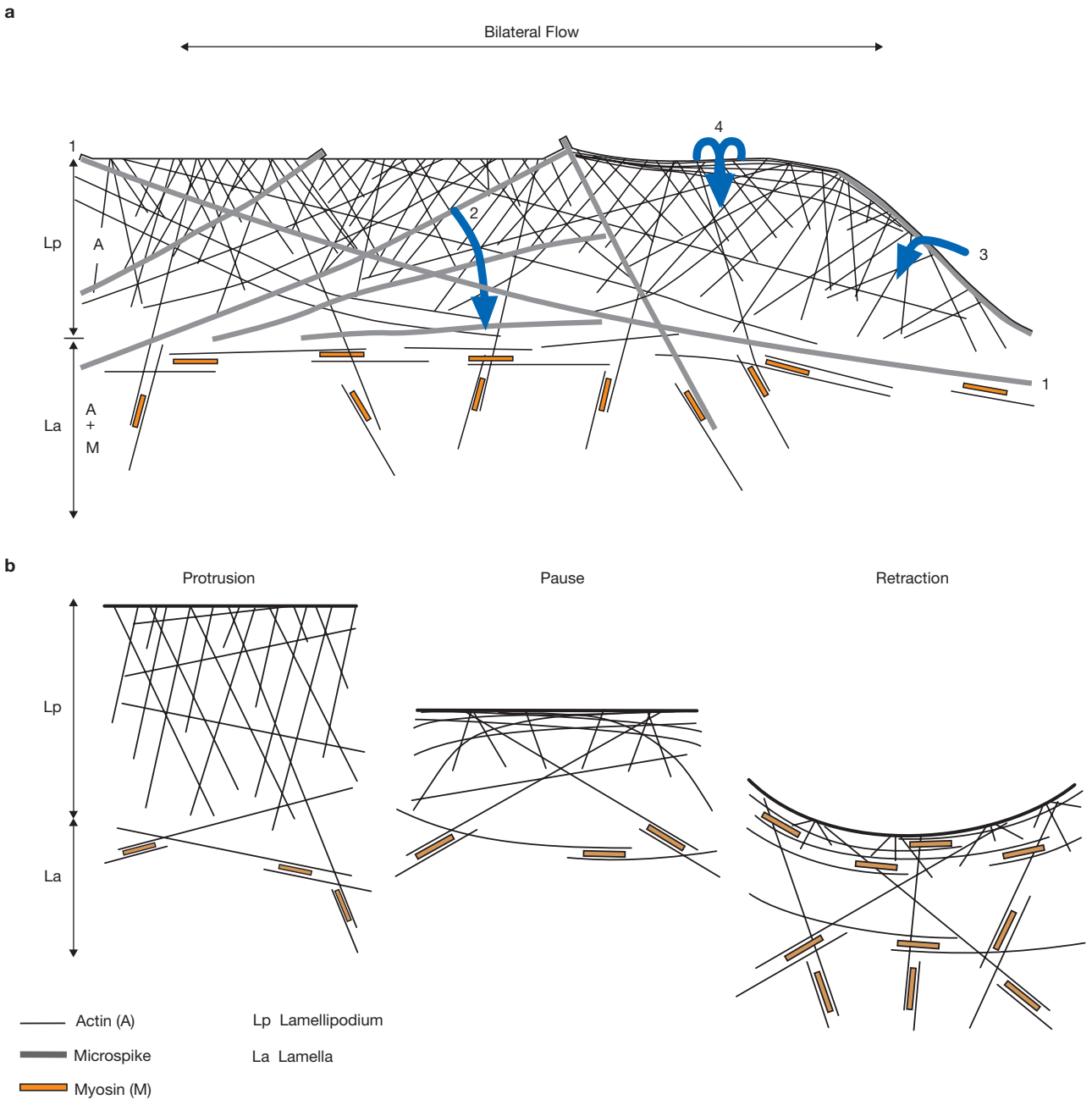


**Figure 5** Filament reorganization during protrusion, pause and retraction. (**a**) Model of actin filament and microspike reorganization within the lamellipodium and their contribution to the lamella. Lp, lamellipodium, containing actin (A) and associated proteins; La, lamella, containing actin, associated proteins and myosin (A + M). Myosin filaments are depicted by orange bars. The variable orientation of individual filaments (black lines) and filament bundles (microspikes; thick, grey lines) results in a variable, bilateral component of polymerization of filament plus-ends along the front edge of the lamellipodium. Models: 1) marks the two ends of a long microspike bundle that contributes actin filaments directly to the lamella; 2) a microspike translating to the right is arrested by a more radial microspike — it dissociates from the cell edge and moves with retrograde flow into the lamella; 3) a microspike bundle can lead a ruffle that propagates laterally along the lamellipodium; 4) a ruffle folding rearwards from the front can generate bundles at the base of the lamellipodium. Myosin engages with the subpopulation of anti-parallel actin filaments generated through bilateral flow, which survives the depolymerization activity of cofilin and other factors present in the lamellipodium. This filament population contributes to the construction of the lamella. (**b**) Scheme of transitions from protrusion to retraction. During persistent protrusion, the orientation of filaments is distributed preferably around higher angles to the cell front, with predominantly linear filaments. Slowing and pause are associated with a variable local reduction in actin polymerization rate at filament plus-ends and with depolymerization from the rear. The slowest-growing filaments retard protrusion and faster growing filaments turn more laterally, adopting curved trajectories. As pause persists, the longer filaments at low angles increase in proportion, due to the preferential loss of the shorter filaments at high angles by depolymerization. Retraction is associated with the recruitment of myosin into the peripheral actin bundle and through linkage of actin filaments into contractile assemblies of the lamella network. The contractile bundle is anchored at both ends into adhesion foci that developed during retraction (not shown). Microspikes also contribute filaments directly to retracting edges (Supplementary Information, Fig. S3a and Movie 3a).

## METHODS

**Correlated light and electron microscopy.** The technique used for correlated light and electron microscopy is described in detail elswhere[1]. In brief, the procedure was as follows. Formvar films cast on a glass slide were floated on a water surface and coverslips (22 × 30 mm) were placed on the film, retrieved on Parafilm and dried. A grid pattern was then embossed on the film by evaporation of gold through tailor-made masks placed on the coverslips. The transfected cells were plated on coverslips coated with laminin (B16) or fibronectin (MTLn3). After video microscopy and fixation, the coverslips were transferred to a 9-cm Petri dish filled with cytoskeleton buffer (CB, 10 mM MES, 150 mM NaCl, 5 mM EGTA, 5 mM glucose, 5 mM $MgCl_2$; pH 6.1) and the film gently peeled off the coverslip with forceps. The film was then inverted and brought to the buffer surface to spread out under surface tension. Under a dissecting microscope, the film was floated on a stainless-steel ring platform and liquid removed until the film was immobilized, with the grid pattern centred. An electron microscopic grid (50 mesh hexagonal, copper) was then placed on the film with the central hole over the region containing the cell of interest. For this manipulation, the grid was mounted in forceps held in a modified Leica dual-pipette holder to allow controlled release, with the pipette holder mounted on a Narashige micromanipulator. The film was then floated off the stand by addition of buffer, recovered with a piece of parafilm, rinsed with negative stain solution and dried on the cell side. The negative stain was composed of a mixture of sodium silicotungstate (2%; Agar Scientific) and aurothioglucose (1%; Wako Chemicals), pH 7.0. Cells were observed and imaged immediately in the electron microscope (FEI Morgagni).

**Cells, constructs and transfection.** B16-F1 mouse melanoma cells were maintained as described previously[2] and transiently transfected using Fugene 6 (Roche), according to the manufacturer's instructions. Cells were transfected with pEGFP–β-actin (BD Biosciences); actin fused to Ruby, a monomeric RFP variant[3]; a mixture of pEGFP–actin and mCherry–VASP; or a mixture of mCherry–actin and PA–GFP–actin. mCherry–VASP was generated by exchanging EGFP in EGFP–VASP[4,5], an improved version of mRFP, kindly provided by Roger Tsien (University of California, San Diego, CA). PA–GFP–actin was made by exchanging EGFP in pEGFP–β-actin (Clontech) for PA–GFP, kindly provided by George Patterson and Jennifer Lippincott-Schwartz (National Institutes of Health, Bethesda, MD). mCherry–actin was kindly provided by Malgorzata Szczodrak (Helmholz Centre for Infection Research, Braunschweig, Germany). The myosin light chain GFP construct and Ruby construct were kindly provided by Rex Chisholm (Nothwestern University, Chicago IL) and Annette Muller-Taubenberger (Ludwig Maximillian University, Munich, Germany), respectively. Carcinoma MTLn3 cells were kindly provided by Jeff Segall (Albert Einstein College of Medicine, New York, NY) and Bob van de Water (Amsterdam Center for Drug Research, Leiden, The Netherlands) and maintained in α-MEM containing ribonucleosides and deoxyribonucleosides, 5% fetal bovine serum (Sigma) and penicillin/streptomycin.

**Live-cell imaging and fixation.** For light microscopy, the film-coverslip combination carrying the cells was mounted in a home made plexiglass flow-through chamber that fitted on a temperature-controlled heating platform (Harvard Instruments). The chamber (40 × 20 × 8 mm) featured two syringe needles glued into each end that connected to a central channel (0.5 mm deep) between the filmed coverslip on the base and an upper, round coverslip glued to a central depression in the chamber.

Imaging was performed on a Zeiss Axiovert 200M inverted microscope equipped with a rear-illuminated, cooled CCD camera (Micromax or Cascade, Roper), together with a filter wheel and shutters controlled with Metamorph software. Halogen lamps were used for imaging in both the phase contrast and fluorescence channels. Images were collected in one or two fluorescent channels and in phase contrast, with 8–15 s between frames (see legends).

Cells were fixed at the end of a selected video sequence by sucking the fixative/detergent mixture through the chamber. For B16 cells, the composition of the mixture was: 0.5% Triton, 0.25% glutaraldehyde in CB, with phalloidin (1 μg $ml^{-1}$) added. For MTLn3 cells, the procedure was the same but with 0.25% Triton and 1% glutaraldehyde. An initial fixation of 2 min in this mixture was followed by a post-fixation in 2% glutaraldehyde (in CB containing 1 μg $ml^{-1}$ phalloidin) for 5–10 min. Final fluorescence images of the selected cell were recorded during the initial fixation period. The coverslip was removed from the chamber and stored in CB containing 2% glutaraldehyde and 10 μg $ml^{-1}$ phalloidin at 4 °C until processing for electron microscopy.

For acquisition of the images displayed in Supplementary Information, Fig. S5a–d and Movie 3, cells were maintained in an open heating chamber (Warner Instruments) at 37 °C, on an inverted microscope (Axiovert 100TV, Zeiss) equipped with a rear-illuminated CCD camera (TE/CCD-1000 TKB, Princeton Instruments) driven by IPLab software (Scanalytics). Images were collected with a time between frames of 12.5 s (Supplementary Information, Fig. S3a) or 18 s (Supplementary Information, Fig. S3b–d).

Experiments with photoactivation of fluorescence were performed on cells co-transfected with PA–GFP–actin and mCherry–actin, using a Zeiss LSM510 laser scanning confocal microscope equipped with argon and helium-neon lasers for fluorescence observation and a diode-UV laser for photoactivation.

**Image analysis and processing.** Electron micrographs were processed in ImageJ using a bandpass filter to equalize the staining density and enhance filament contrast. For filament counts and angle measurements, a line of 1 μm (B16 cells) or 0.5 μm (MTLn3 cells) was drawn parallel to the cell edge using Adobe Photoshop; filaments crossing this line were overlaid with short lines and the angles between these lines and the cell edge measured in Photoshop.

Fluorescence intensities were measured with the linescan tool of Metamorph (Molecular Devices). For velocity measurements, sequential GFP–actin images were processed with the 'detect edges' filter in Metamorph. The position of the peak value of a line scan across the lamellipodium was used to define the position of the cell edge and the velocity was calculated from one frame to the next. Regression curves were drawn with Microsoft Excel.

*Note: Supplementary Information is available on the Nature Cell Biology website.*

ACKNOWLEDGEMENTS

The authors thank the Human Frontier Science Program Organization (HFSPO), The Austrian Science Research Council (FWF) and the Vienna Science Research and Technology Fund (WWTF) as well as the City of Vienna/Zentrum für Innovation und Technologie via the Spot of Excellence grant 'Center of Molecular and Cellular Nanostructure' for financial support. K.R. was supported in part by grants from the Deutsche Forschungsgemeinschaft (SPP1150 and FOR629). We also thank Guenter Resch for the electron microscope facility management and advice with image processing, Tibor Kulcsar and Hannes Tkadletz for graphics and Natalia Andreyeva for helpful comments. The authors thank Roger Tsien, Annette Muller-Taubenberger, Malgorzata Szczodrak, George Patterson, Jennifer Lippincott-Schwarz and Rex Chisholm for probes, and Jeff Segall and Bob van de Water for MTLn3 cells.

Published online at http://www.nature.com/naturecellbiology/
Reprints and permissions information is available online at http://npg.nature.com/reprintsandpermissions/

1. Abercrombie, M., Heaysman, J. E. & Pegrum, S. M. The locomotion of fibroblasts in culture. II. 'Ruffling'. *Exp. Cell Res.* **60,** 437–444 (1970).
2. Ponti, A., Machacek, M. S., Gupton, L., Waterman-Storer, C. M. & Danuser, G. Two distinct actin networks drive the protrusion of migrating cells. *Science* **305,** 1782–1786 (2004).
3. Svitkina, T. M. & Borisy, G. G. Arp2/3 complex and actin depolymerizing factor/cofilin in dendritic organization and treadmilling of actin filament array in lamellipodia. *J. Cell Biol.* **145,** 1009–1026 (1999).
4. Small, J. V., Stradal, T., Vignal, E. & Rottner, K. The lamellipodium: where motility begins. *Trends Cell Biol.* **12,** 112–20 (2002).
5. Small, J. V., Isenberg, G. & Celis, J. E. Polarity of actin at the leading edge of cultured cells. *Nature* **272,** 638–639 (1978).
6. Small, J. V., Herzog, M. & Anderson, K. Actin filament organization in the fish keratocyte lamellipodium. *J. Cell Biol.* **129,** 1275–1286 (1995).
7. Pollard, T. D. & Borisy, G. Cellular motility driven by assembly and disassembly of actin filaments. *Cell* **112,** 453–465 (2003).
8. Pollard, T. D. Regulation of actin filament assembly by arp2/3 complex and formins. *Annu. Rev. Biophys. Biomol. Struct.* **36,** 451–477 (2007).
9. Heath, J. P. & Holifield, B. F. On the mechanisms of cortical actin flow and its role in cytoskeletal organisation of fibroblasts. *Symp. Soc. Exp. Biol.* **47,** 35–56 (1993).
10. Rottner, K., Behrendt, B., Small, J. V. & Wehland, J. VASP dynamics during lamellipodia protrusion. *Nature Cell Biol.* **1,** 321–322 (1999).
11. Condeelis, J. & Segall, J. E. Intravital imaging of cell movement in tumours. *Nature Rev. Cancer* **3,** 921–930 (2003).
12. Small, J. V. & Resch, G. P. The comings and goings of actin: coupling protrusion and retraction in cell motility. *Curr. Opin. Cell Biol.* **17,** 517–523 (2005).

13. Medeiros, N. A., Burnette, D. T. & Forscher, P. Myosin II functions in actin-bundle turnover in neuronal growth cones. *Nature Cell Biol.* **8,** 215–226 (2006).
14. Small, J. V. The actin cytoskeleton. *Electron Microsc. Rev.* **1,** 155–174 (1988).
15. Abraham, V. C., Krishnamurthi, V., Taylor, D. L. & Lanni, F. The actin-based nanomachine at the leading edge of migrating cells. *Biophys. J.* **77,** 1721–1732 (1999).
16. Kozlov, M. M. & Bershadsky, A. D. Processive capping by formin suggests a force-driven mechanism of actin polymerization. *J. Cell Biol.* **167,** 1011–1017 (2004).
17. Carlier, M. F. & Pantaloni, D. Control of actin assembly dynamics in cell motility. *J. Biol. Chem.* **282,** 23005–23009 (2007).
18. Mogilner, A. On the edge: modeling protrusion. *Curr. Opin. Cell Biol.* **18,** 32–39 (2006).
19. Fisher, G. W., Conrad, P. A., DeBiasio, R. L. & Taylor, D. L. Centripetal transport of cytoplasm, actin, and the cell surface in lamellipodia of fibroblasts. *Cell Motil. Cytoskeleton* **11,** 235–247 (1988).
20. Vallotton, P., Danuser, G., Bohnet, S., Meister, J. J. & Verkhovsky, A. B. Tracking retrograde flow in keratocytes: news from the front. *Mol. Biol. Cell* **16,** 1223–1231 (2005).
21. Hotulainen, P. & Lappalainen, P. Stress fibers are generated by two distinct actin assembly mechanisms in motile cells. *J. Cell Biol.* **173,** 383–394 (2006).
22. Blanchoin, L., Pollard, T. D. & Hitchcock-DeGregori, S. E. Inhibition of the Arp2/3 complex-nucleated actin polymerization and branch formation by tropomyosin. *Curr. Biol.* **11,** 1300–1304 (2001).
23. Pollard, T. D., Blanchoin, L. & Mullins, R. D. Actin dynamics. *J. Cell Sci.* **114,** 3–4 (2001).
24. Amann, K. J. & Pollard, T. D. Direct real-time observation of actin filament branching mediated by Arp2/3 complex using total internal reflection fluorescence microscopy. *Proc. Natl Acad. Sci. USA.* **98,** 15009–15013 (2001).
25. Mullins, R. D., Heuser, J. A. & Pollard, T. D. The interaction of Arp2/3 complex with actin: nucleation, high affinity pointed end capping, and formation of branching networks of filaments. *Proc. Natl Acad. Sci. USA.* **95,** 6181–6186 (1998).
26. Resch, G. P., Goldie, K. N., Hoenger, A., & Small, J. V. Pure F-actin networks are distorted and branched by steps in the critical-point drying method. *J. Struct. Biol.* **137,** 305–312 (2002).
27. Medalia, O., Weber, I., Frangakis, A. S., Nicastro, D., Gerisch, G. & Baumeister, W. Macromolecular architecture in eukaryotic cells visualized by cryoelectron tomography. *Science.* **298,** 1209–1213 (2002).
28. Gupton, S. L. *et al.* Cell migration without a lamellipodium: translation of actin dynamics into cell movement mediated by tropomyosin. *J. Cell Biol.* **168,** 619–631 (2005).
29. Giannone, G. *et al.* Lamellipodial actin mechanically links myosin activity with adhesion-site formation. *Cell* **128,** 561–575 (2007).
30. Hebert, B., Costantino, S. & Wiseman, P. W. Spatiotemporal image correlation spectroscopy (STICS) theory, verification, and application to protein velocity mapping in living CHO cells. *Biophys. J.* **88,** 3601–3614 (2005).

nature cell biology



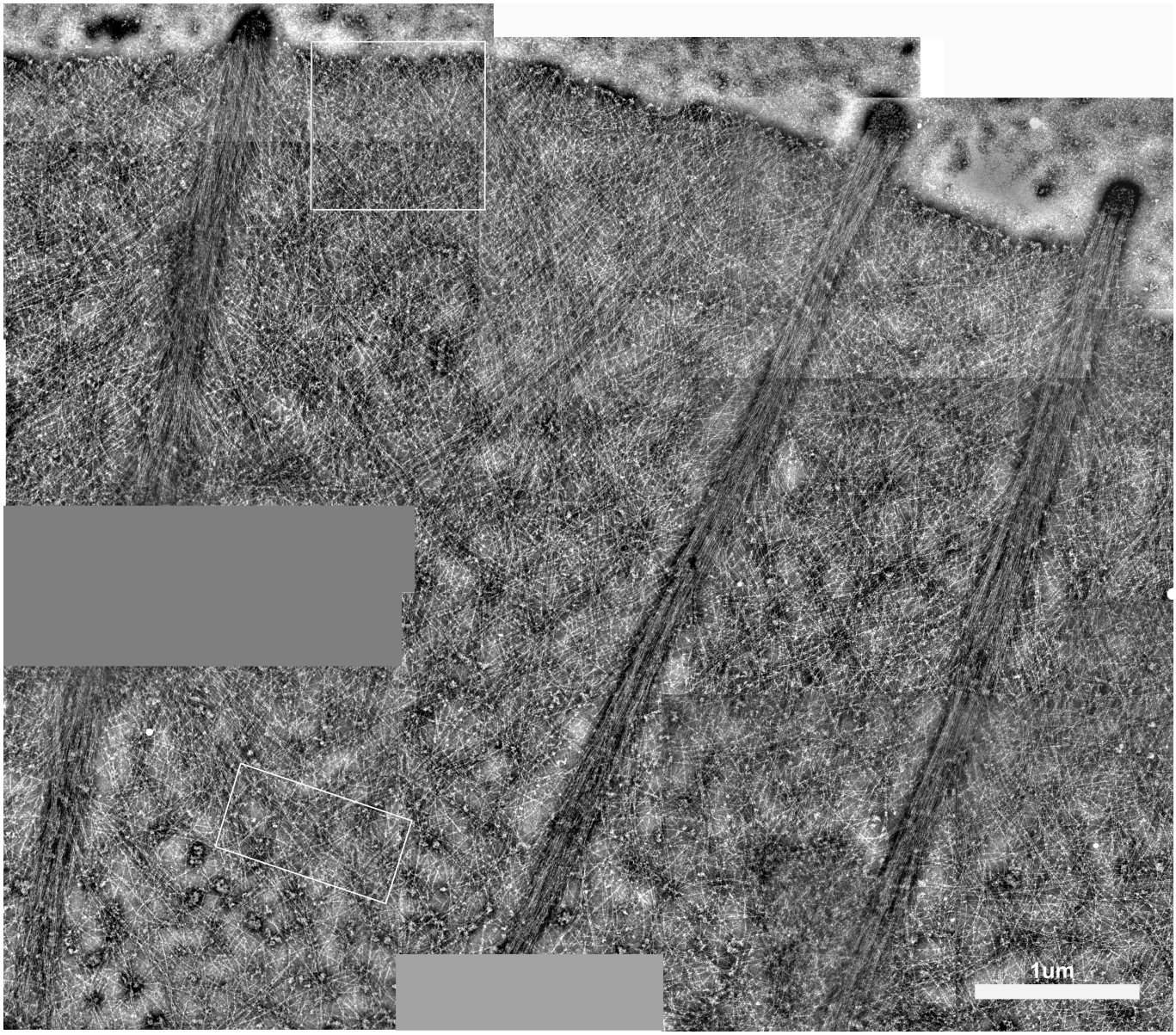


**Figure S1** Electron micrograph overview of the region corresponding to Fig. 1c, with the positions of Figs. 2a and b boxed.

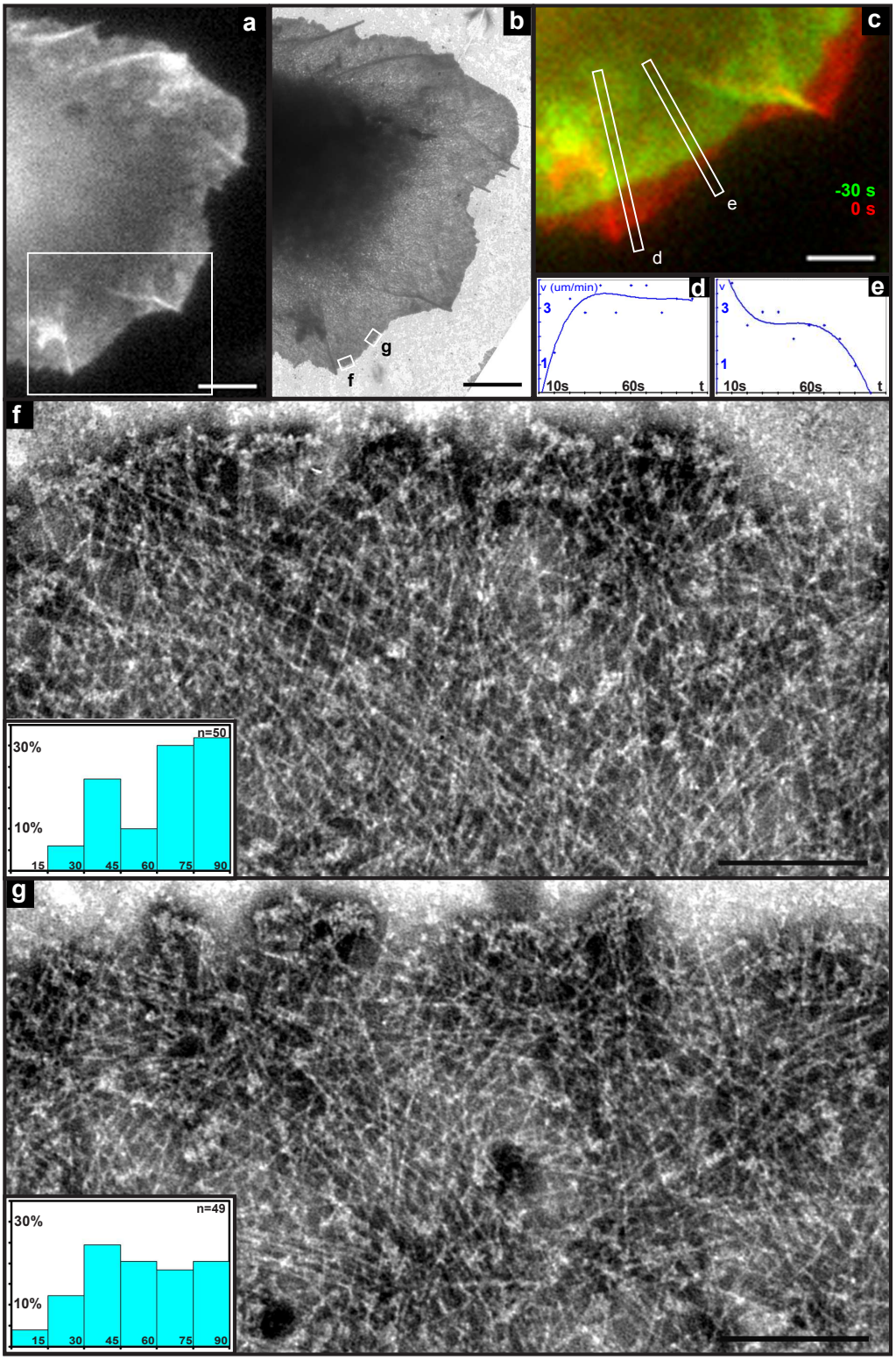


**Figure S2** Transition from protrusion to pause in MTLn3 cell lamellipodia. a, video frame, prior to fixation, of an MTLn3 cell transfected with EGFP-actin. b, overview of the fixed and stained cell in the electron microscope. c, region of the cell boxed in a, with the last video frame before fixation (red) overlayed with the frame 30 seconds before (green) to show the relative degrees of protrusion along the lamellipodium segment. d and e show the velocity traces of the cell edge for the corresponding positions marked in "c" by the white rectangles. f and g, electron micrographs of the positions shown in the overview b and corresponding to the cell edge positions d and e in c. Histograms in f and g show the angular distribution of filaments measured at 200 nm from the cell edge. Counts were made along 0.5 µm lines drawn parallel to the cell edge, to avoid overlap with adjacent zones. Bars, a,b, 5 µm; c, 3 µm; f, g, 200 nm.

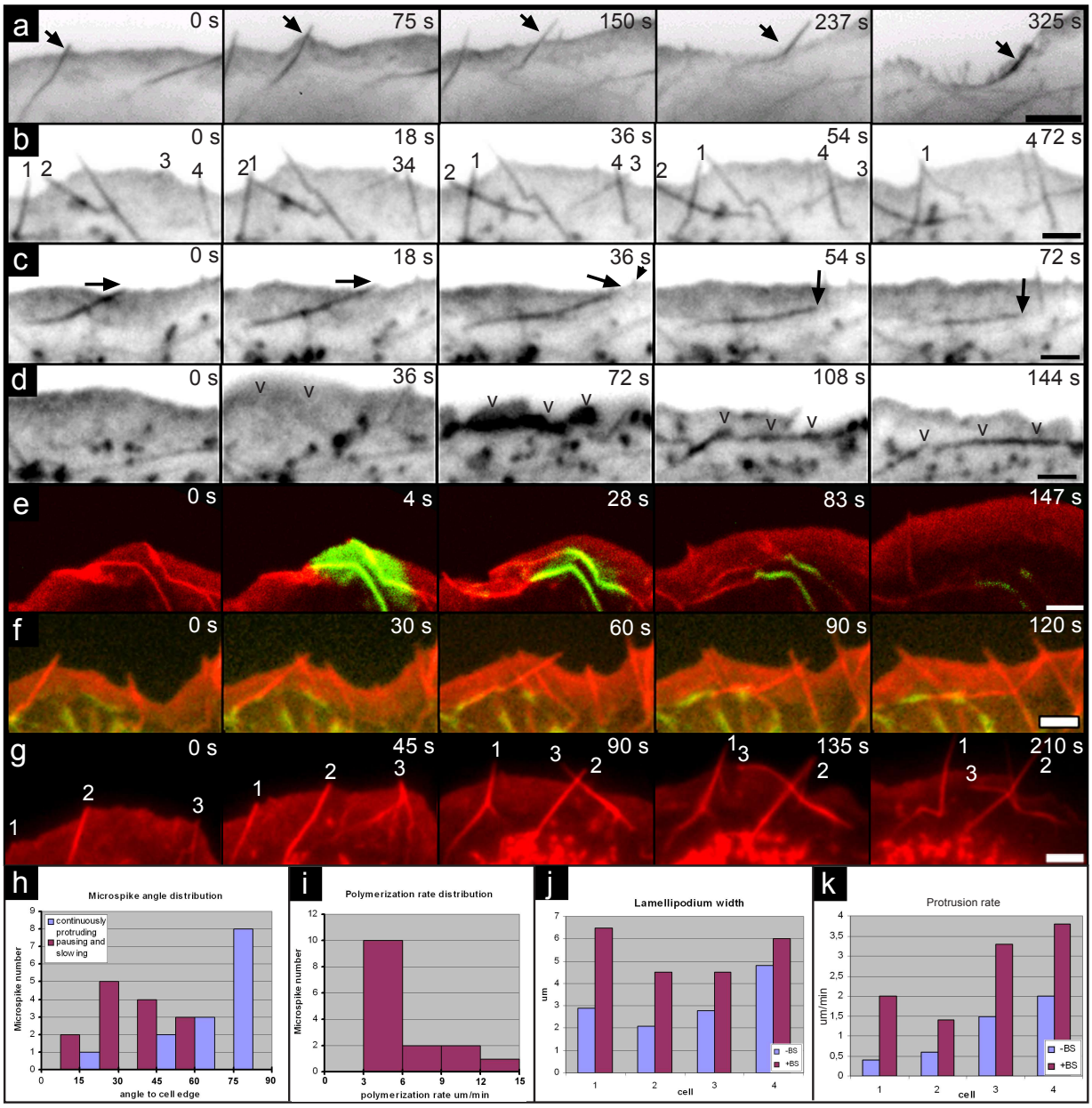


**Figure S3** Bi-lateral flow of microspike bundles along the lamellipodium results in the contribution of bipolar arrays of actin filaments to the lamella. a. Video sequence of a lamellipodium segment of a B16 melanoma cell transfected with actin-GFP showing contribution of a laterally translating microspike to the construction of a retracting edge that forms in the last frame (arrow). This and the following sequences (b-d) are shown in negative contrast. All times are in seconds. Bar, 4 µm. b-d, selected frames of video sequences of the same region of a B16 melanoma cell expressing Ruby-actin. b shows two pairs of microspike bundles (numbered 1-4) crossing during the sequence (at 18 and 36 s). c, the tip of a laterally translating, long microspike (arrow) is stopped by a small radial microspike at 36 s (arrowhead), leading to dissociation of the long microspike from the lamellipodium tip and retrograde flow of the remaining bundle to the base. d, generation of an actin bundle parallel to the base of the lamellipodium (144 s) from a ruffle (v) that folds rearwards from the front (36-108 s), without a microspike. Bars, 2 µm. e. Lamellipodium segment of a B16 melanoma cell transfected with mCherry-actin and photoactivatable GFP-actin. The PA-GFP was photoactivated at 4 s. Note contribution of microspike bundles to the lamella as well as the continued turnover of actin. The time between frames after photoactivation was 8 s. Bar, 3 µm. f. Engagement of myosin at base of lamellipodium. Selected video frames of B16 melanoma cell expressing mCherry-actin and GFP-myosin regulatory light chain. Note again bi-lateral translation of microspike bundles and their contribution to bundles at the base of the lamellipodium, where myosin is recruited. Bar, 3 µm. g. Myosin is not required for the lateral translation of microspikes. Frames of a video sequence of a B16 melanoma cell expressing mCherry-actin that was treated with 50 µM blebbistatin. Numbers indicate translating microspikes; time in seconds; bar, 3µm. h, i. Angular distribution and growth rate of microspikes in B16 melanoma cells. h, comparison of microspike angles (to the cell edge) in pausing or slowing cells (purple bars) as compared to fast moving cells (blue bars). 14 microspikes each measured in 5 slow cells and 3 fast cells. i, distribution of actin polymerization rates in microspikes measured using photoactivatable GFP-actin in cells co-transfected with mCherry-actin (as for e). The rate was determined from the extension of microspikes from the point of photoactivation. j, k. Data from 4 cells on the effect of 50-100 µM blebbistatin (BS) on lamellipodium width and protrusion rate in B16 melanoma cells. Within 2-10 minutes of blebbistatin treatment, the extended width of the lamellipodium increased by 15-100% (j) and the protrusion rate by at least two fold (k)

**Supplementary movie legends**

**Movie S1** Video Fig.1, including actin-GFP image after fixation. Time between frames was 8s.

**Movie S2** Video Fig.3. Time between frames was 8s.

**Movie S3** Video Fig. S5.

**Movie S4** Simulation of slowing, pause and retraction in a lamellipodium. During slowing to pause, filaments show a varied reduction in polymersation rate (red and yellow plus ends), resulting in the faster filaments (red) adopting curved trajectories, culminating in a subpopulation of filaments parallel to the cell edge. Slower polymerising filaments (yellow to green) act as tethers and restrain protrusion. Shorter filaments at high angles depolymerise first, leaving longer filaments in antiparallel arrays to recruit myosin (orange bars) for retraction. Microspike bundles also contribute filaments to retracting edges (not depicted).

**Supplementary references**

1. Auinger, S., and J.V. Small. 2007. Correlated light and electron microscopy of the actin cytoskeleton. *Methods in Cell Biology*. in press.
2. Rottner, K., B. Behrendt, J.V. Small, and J. Wehland. 1999. VASP dynamics during lamellipodia protrusion. *Nat Cell Biol*. 1:321-2.
3. Muller-Taubenberger, A., M.J. Vos, A. Bottger, M. Lasi, F.P. Lai, M. Fischer, and K. Rottner. 2006. Monomeric red fluorescent protein variants used for imaging studies in different species. *Eur J Cell Biol*. 85:1119-29.
4. Carl, U.D., Pollmann, M, Orr, E., Gertler, F.B., Chakraborty, T and Wehland, J. 1999. Aromatic and basic residues within the EVH1 domain of VASP specify its interaction with proline-rich ligands. Curr. Biol. 9:715-8.
5. Shaner, N.C., Campbell, R.E., Steinbach, P.A., Giepmans, B.N.G., Palmer, A.E. and Tsien, R.Y. 2004. Improved monomeric red, orange and yellow fluorescent proteins derived from *Discosoma* sp. red fluorescent protein. Nature Biotechnology 22:1567-72.